Miniaturized all-optical photoacoustic microscopy based on microelectromechanical systems mirror scanning

Article *in* Optics Letters · October 2012

DOI: 10.1364/OL.37.004263 · Source: PubMed

6 authors, including:

Sung-Liang Chen
UM-SJTU Joint Institute, Shanghai Jiao Tong University
40 PUBLICATIONS **909** CITATIONS

SEE PROFILE

Zhixing Xie
University of Michigan
30 PUBLICATIONS **647** CITATIONS

SEE PROFILE

Tao Ling
University of Michigan
75 PUBLICATIONS **1,286** CITATIONS

SEE PROFILE

Lingjie Jay Guo
University of Michigan
439 PUBLICATIONS **16,021** CITATIONS

SEE PROFILE

Miniaturized all-optical photoacoustic microscopy based on microelectromechanical systems mirror scanning

Sung-Liang Chen,[1,†] Zhixing Xie,[1,†] Tao Ling,[2] L. Jay Guo,[2] Xunbin Wei,[3] and Xueding Wang[1,*]

[1]*Department of Radiology, University of Michigan, Ann Arbor, Michigan 48109, USA*

[2]*Department of Electrical Engineering and Computer Science, University of Michigan, Ann Arbor, Michigan 48109, USA*

[3]*Med-X Research Institute, Shanghai Jiao Tong University, Shanghai 200030, China*

**Corresponding author: xdwang@umich.edu*

Received August 6, 2012; accepted August 31, 2012;
posted September 12, 2012 (Doc. ID 173862); published October 11, 2012

Achieving photoacoustic microscopic imaging through a miniaturized scanning head is a crucial step toward high-resolution photoacoustic endoscopy. In this work, we have developed a miniaturized probe head using a microelectromechanical systems (MEMS) based mirror for raster scan of the laser beam and our newly developed super broad bandwidth microring resonator based ultrasound detector for photoacoustic signal detection. Through this all-optical design, which offers unique advantages for endoscopic applications, this system is capable of three-dimensional (3D) imaging with high resolution of 17.5 μm in lateral direction and 20 μm in axial direction at a distance of 3.7 mm. After the performance of this system was validated through the experiments on printed grids and a resolution test target, microscopic imaging of the 3D microvasculatures in canine bladders was also conducted successfully, demonstrating the potential of novel photoacoustic endoscopic in future clinical management of bladder cancer.

OCIS codes: 170.3880, 170.5120, 180.5810.

A majority of cancers originate in the epithelial tissues of the human body, including those in the oral cavity and pharynx, digestive system, respiratory system, genital system, and urinary system. For example, bladder cancer is the fifth leading new cancer diagnosis in the United States and is fourth among men [1]. The long-term survival and the need for lifelong routine monitoring and treatment lead to a cost per patient for bladder cancer that is the highest among all cancers [2,3]. Despite the advances in diagnosis and therapy in the past decades, bladder cancer remains an important public health problem. One of the major reasons is the lack of powerful screening and diagnostic technology.

Photoacoustic imaging (PAI) is an emerging modality and has great potential for *in vivo* biomedical applications [4]. It provides image information of optical-absorption contrast or functional properties by detecting ultrasonic waves, generated based on thermoacoustic effect. It has been demonstrated that a potential marker to obtain prognostic information about bladder cancer is tumor neoangiogenesis [5], which can be quantified by morphometric characteristics, such as microvascular density. Photoacoustic microscopy (PAM), by rendering three-dimensional (3D) map of microvasculature with unbeatable sensitivity and high resolution, holds promise for evaluation of neoangiogenesis associated with bladder cancer generation and progression [6]. To achieve *in vivo* noninvasive evaluation of a bladder tumor with microscopic resolution, the best method is to perform PAI in an endoscopic manner, similar to conventional white light cystoscopy. However, despite the rapid advancement of PAI technology in the past decade, achieving high-resolution endoscopic imaging with PAI is still very challenging and in need of development. One reason is that most current PAI systems are usually bulky and do not have sufficient detection bandwidth required for microscopic resolution.

Miniaturized probes for PAI have been studied recently [7–10]. Mechanical scanning based on micromotor and a single transducer can acquire only two-dimensional (2D) and side-view images [7]. Another design using a taper reflector and a ring transducer array suffers from poor transverse resolution [8]. We expect that applying microelectromechanical systems (MEMS) mirrors capable of 2D scanning is the best way to enable forward-view scanning [9] and high-resolution imaging [11]. In this work, we demonstrate feasibility to miniaturize the probe head of a PAM system without sacrificing the image quality, by using a MEMS mirror for fast scanning. In this system, an optical microring resonator with a noise equivalent detectable pressure (NEDP) of 29 Pa is employed for sensitive ultrasound detection [12]. The detection mechanism has been introduced before in the literature [13]. Optical detection of photoacoustic signals leads to a very unique all-optical design. The advantages of the microring resonator, including small size, super broad bandwidth, size-independent sensitivity, and free from electromagnetic interference, particularly benefit the design of an endoscopic probe. Moreover, to gain enough signal-to-noise ratio, the piezoelectric transducer used in conventional PAM systems should connect directly to an amplifier circuit/system before the signal is routed to the data acquisition board. This creates significant challenge for endoscopic application imposed by the limited space constraints. In contrast, microring sensors with optical fiber connections eliminate the signal routing and delivery problem easily by using external high-speed and high-gain photodetectors.

The schematic of the system is shown in Fig. 1(a). A diode-pumped solid-state Nd:YAG laser (SPOT-10-200-532, Elforlight Ltd., UK) is employed to provide pulses of 2 ns duration at wavelength of 532 nm. The laser beam is coupled into a fiber (SMF-28e+, Thorlabs, Newton, New Jersey) by a focusing lens, and is delivered to a MEMS tilt

0146-9592/12/204263-03$15.00/0

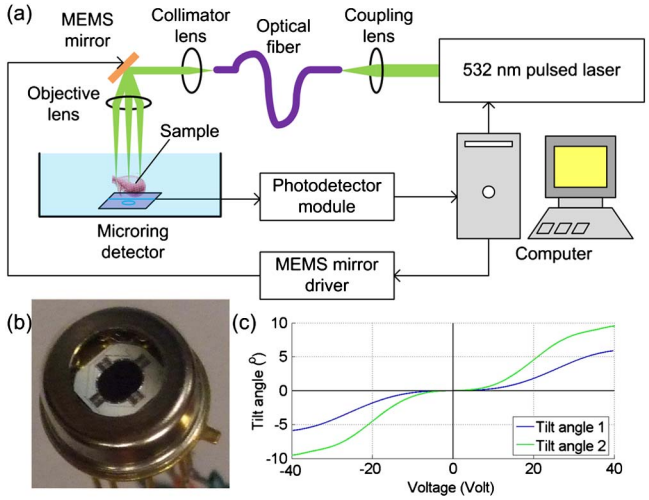

Fig. 1. (Color online) (a) Schematic of MEMS-based PAM system. (b) A photograph of the MEMS mirror. (c) The calibrated response of mirror tilt angle versus applied voltages.

mirror (TM-2520, Sercalo Microtechnology Ltd., Switzerland) with a laser spot size of 1 mm after a collimator. The MEMS mirror is used to perform 2D scanning of laser beam. Figure 1(b) shows a photograph of the MEMS mirror. An aspheric lens (A220-A, Thorlabs) is used as an objective lens. The diameter of the commercial MEMS mirror and the objective lens is 9.2 and 7.2 mm, respectively. A MEMS driver board provided by Sercalo Ltd. is used to control the mirror tilt angle. A digital-to-analog converter in the driver board delivers voltages to set the angle using electrostatic actuation. 2D scanning is realized by setting different voltages of two pairs of electrodes, which is used to control two-axis tilt. Figure 1(c) shows calibrated response of tilt angle versus applied voltages. Compared with our previous all-optical PAM system [12], a fiber-optic pulsed laser delivery, a MEMS mirror, and a small objective lens are adopted in the current system to meet the needs of miniaturization.

In this system, the laser works in an external trigger mode. An output trigger signal is used to synchronize the laser triggering, the MEMS tilt, and the data acquisition. Laser-generated photoacoustic signal is received by a microring detector, which is placed under the sample and works on a transmission mode. The microring resonator with a ring diameter of 60 μm is a wideband single-element ultrasound detector with a measured receiving bandwidth up to ~100 MHz [12]. The photoacoustic signal modulated optical signal from the microring is detected by a photoreceiver module (1801-FC-AC, New Focus). The detected signal is then digitized at a sampling rate of 200 MHz for 2.5 μs and stored by a data acquisition board in a PC. The microring resonator is kept stationary during laser scanning and no signal averaging is needed.

We have acquired images from both phantom and *ex vivo* tissue specimens to demonstrate the ability of the imaging system. Given the 11 mm focal length of the objective lens and the maximum tilt angles of the MEMS mirror (±6° and ±9° for the two axes, respectively), the system is able to cover an area of up to 2.3 mm× 3.5 mm. To obtain an equi-interval stepping size, the input voltages are set according to the calibrated nonlinear response in Fig. 1(c). Due to the 50 Hz limit of the MEMS driver board, a 2D raster scan of 256 × 256 steps takes almost half an hour, which also includes the data transfer time. However, as we know, a MEMS mirror with step response setting times <100 μs is commercially available, which can drastically improve the imaging speed.

Figure 2 shows the imaging results of phantoms. We placed the microring detector at ~3.7 mm under the phantom surface. Both phantom and the detector were immersed in the deionized water for acoustic coupling. A black mesh grid printed on a transparency with a designed gap size of 381 μm was imaged. The scanning area was 1 mm × 1 mm. The maximum amplitude projection (MAP) image was presented in Fig. 2(a). The sizes of the grids measured in the image were in the range of 360–390 μm, showing a good agreement with the designed grid size. Figure 2(b) presents a typical A-line signal and its amplitude after the Hilbert transform (envelope). We determined the axial resolution using the criteria of the FWHM. The quantified axial resolution is better than 20 μm at a detection distance of 3.7 mm. The good axial resolution is benefited from the wide bandwidth of the microring resonator. Higher axial resolution can also be achieved by reducing the sound propagation distance [12].

To quantify the system lateral resolution, we imaged a USAF 1951 resolution test target (T-20-P-TM, Applied Image, Rochester, New York). The MAP image of the resolution target was shown in Fig. 2(c). Figure 2(d) showed the one-dimensional (1D) profile measured along the line as marked in Fig. 2(c). Spatial averaging over ~12 pixels, as indicated by the bar in Fig. 2(c), was applied to improve the contrast-to-noise ratio (CNR) in Fig. 2(d). The smallest resolvable bar spacing is 17.5 μm (group 5, element 6), which indicates the lateral resolution is better than 17.5 μm. Since the same detector is used in our current and previous system [12], the NEDP and axial resolution are expected to be similar. The lateral resolution and imaging speed are worse in the current system. However, the former can be improved by increasing the NA of the objective lens and the latter can be increased

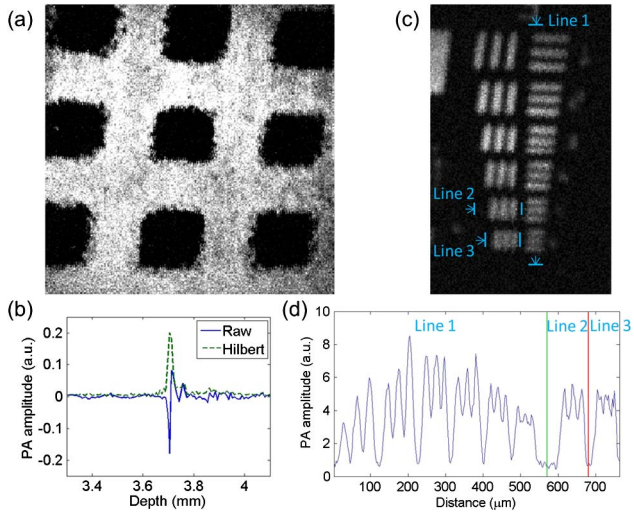

Fig. 2. (Color online) (a) MAP image of a printed mesh grid. (b) A-line photoacoustic signal and its amplitude after the Hilbert transform. (c) The MAP image of a USAF resolution test target. (d) 1D profile plotted along the lines marked in (c).

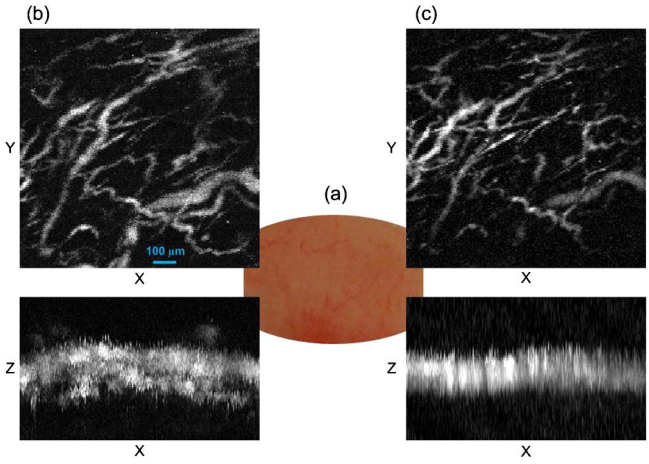

Fig. 3. (Color online) (a) Anatomical photograph of the inner wall of a canine bladder. (b) MAP images on the XY and XZ planes of the microvasculature in the bladder wall obtained by microring detectors. (c) MAP images of the same area acquired by the needle hydrophone. All images share the same scale bar as shown in the left-upper image.

by using a MEMS mirror with fast response time, as mentioned above.

To evaluate the performance of this system in imaging biological tissues, fresh canine bladders were employed. This study on canine bladder model also helps to explore the potential of adapting the novel PAM technique to bladder cancer diagnosis. Before the imaging experiment, the harvested whole bladder was kept fresh in a refrigerator. The laboratory animal protocol for this work was approved by the UCUCA of the University of Michigan. Figure 3(a) shows an anatomical photograph of the excised inner wall of the bladder.

Other than imaging using the microring resonator, we also acquired images from the same sample using a needle hydrophone for comparison with the results from the microring resonator. The highly sensitive custom-built needle hydrophone has a center frequency of 35 MHz and a −6 dB bandwidth of 100%. The needle hydrophone was operated on the reflection mode, while the microring detector worked in the transmission mode. In this way, the same area in the same sample can be scanned with the microring resonator and the hydrophone simultaneously, facilitating a better comparison. The MAP images showing the microvasculature in the canine bladder obtained by the microring resonator and the hydrophone are shown in Figs. 3(b) and 3(c), respectively. The maximum CNRs are similar: 32 dB for Fig. 3(b) and 33 dB for Fig. 3(c). Larger field of view was obtained by the microring resonator because of its small active element size (60 μm) compared with that of the needle hydrophone (~1 mm). The MAP image on the XZ plane acquired by the hydrophone shows obscure features along the axial direction, which is due to relatively narrower bandwidth and, as a result, worse axial resolution associated with the needle hydrophone. In contrast, at least two layers of tissue features can be recognized along the Z direction in the MAP image on the XZ plane obtained by the microring resonator.

In this work, we have demonstrated a miniaturized PAM probe head capable of optical-resolution PAI. As demonstrated by the results from phantoms and *ex vivo* tissues, this system based on the MEMS mirror scanning and the microring detector shows satisfactory image quality. High resolution of 17.5 μm in lateral direction and 20 μm in axial direction have been achieved. Microvasculatures in canine bladders have also been mapped with good spatial resolution, high CNR, and satisfactory continuity, suggesting the potential of PAM in diagnostic imaging and guided treatment of bladder cancer and other epithelial cancers.

However, before a clinically usable endoscopic PAM system could be fabricated, several technical problems still need to be resolved. First, a MEMS mirror with smaller element size in the range of 3–5 mm is needed if the targeted probe size is less than 7 mm (comparable to commercial cystoscopic catheters). We also expect that the MEMS mirror could allow wider scanning angle for larger imaging area and faster scanning speed, both major concerns in clinical application of an endoscopic system. Second, we are also trying to build a microring resonator that is optically transparent at the wavelength of the pulsed laser for photoacoustic signal generation. With such a design, the scanning laser beam can go through the microring resonator without being interfered, facilitating a reflection mode PAM. As demonstrated in our previous study, building an optically transparent microring resonator is feasible, by using a transparent silica substrate [10].

This work was supported by the National Institutes of Health under grants R01AR060350 and R01AR055179, University of Michigan-Shanghai Jiao Tong University (UM-SJTU) Joint Grant, and Basic Radiological Sciences (BRS) Grant Award G012284.

†These authors contributed equally to this work

References

1. A. Jemal, R. Siegel, J. Xu, and E. Ward, CA-Cancer J. Clin. **60**, 277 (2010).
2. E. B. C. Avritscher, C. D. Cooksley, H. B. Grossman, A. L. Sabichi, L. Hamblin, C. P. Dinney, and L. S. Elting, Urology **68**, 549 (2006).
3. M. F. Botteman, C. L. Pashos, A. Redaelli, B. Laskin, and R. Hauser, Pharmacoeconomics **21**, 1315 (2003).
4. L. V. Wang, ed., in *Photoacoustic Imaging and Spectroscopy* (Taylor & Francis/CRC Press, 2009).
5. Y.-K. Zee, J. P. B. O'Connor, G. J. M. Parker, A. Jackson, A. R. Clamp, M. B. Taylor, N. W. Clarke, and G. C. Jayson, Nat. Rev. Urol. **7**, 69 (2010).
6. B. H. Bochner, R. J. Cote, N. Weidner, S. Groshen, S.-C. Chen, D. G. Skinner, and P. W. Nichols, J. Natl. Cancer Inst. **87**, 1603 (1995).
7. J.-M. Yang, K. Maslov, H.-C. Yang, Q. Zhou, K. K. Shung, and L. V. Wang, Opt. Lett. **34**, 1591 (2009).
8. Y. Yuan, S. Yang, and D. Xing, Opt. Lett. **35**, 2266 (2010).
9. L. Xi, J. Sun, Y. Zhu, L. Wu, H. Xie, and H. Jiang, Biomed. Opt. Express **1**, 1278 (2010).
10. S.-L. Chen, T. Ling, H. W. Baac, and L. J. Guo, Proc. SPIE **7899**, 78992T (2011).
11. J. Yao, C.-H. Huang, L. Wang, J.-M. Yang, L. Gao, K. I. Maslov, J. Zou, and L. V. Wang, J. Biomed. Opt. **17**, 080505, (2012).
12. Z. Xie, S.-L. Chen, T. Ling, L. J. Guo, P. L. Carson, and X. Wang, Opt. Express **19**, 9027 (2011).
13. C.-Y. Chao, S. Ashkenazi, S.-W. Huang, M. O'Donnell, and L. J. Guo, IEEE Trans. Ultrason. Ferroelectr. Freq. Control **54**, 957 (2007).